



Economical preparation of high-performance activated carbon fiber papers as self-supporting supercapacitor electrodes

Junjun Chen ^{a,b}, Junxian Xie ^a, Charles Q. Jia ^b, Chenying Song ^a, Jian Hu ^a, Hailong Li ^{a,*}

^a School of Light Industry and Engineering, South China University of Technology, Guangzhou, CN 510640, China

^b Department of Chemical Engineering and Applied Chemistry, University of Toronto, Toronto M5S, Canada



ARTICLE INFO

Keywords:

Paper-based electrode
Papermaking
Carbon fibers
Supercapacitor
Activation

ABSTRACT

The cellulose-based paper electrode has attracted increasing attention for wearable and portable electronic devices. However, the loading of expensive electroactive substances, a large proportion of cellulose matrix and the loss of mechanical flexibility limit its commercial application. This article reports a facile and economical strategy for fabricating high-performance cellulose-based activated carbon fiber papers (ACFPs), which can be used as self-supporting supercapacitor electrodes without any binder. Combining wet papermaking, thermal carbonization, and double activation, the new strategy enables the in-situ transformation of fibrillated pulp fibers into cellulose-derived activated carbon fused with carbon fibers (CFs). The resulting ACFPs are characteristic of high specific surface area (808–1106 m²/g), high conductivity (1640–1786 S/m), prominent tensile strength (4.6–6.4 MPa), and flexible processability. Furthermore, the ACFP exhibits maximum specific capacitance of 48.8F/cm³ (or 165F/g) based on the whole electrode and possesses superior cycling stability. Moreover, electroactive materials are readily loaded onto the ACFPs to enhance the capacitance further. In the ACFPs, the cellulose-derived activated carbon is primarily responsible for capacitive energy storage, while CFs serve as a highly functional network due to their low thermal expansion coefficient and high electrical conductivity. Overall, this work provides a novel strategy for manufacturing scalable, cost-effective paper-based electrode materials with broad application prospects in energy storage.

1. Introduction

With the development of wearable and portable electronic devices, it is essential to develop light, thin and flexible materials with excellent electrochemical performance [1–4]. Paper-based supercapacitors entail unprecedented scientific interest due to their high power density, fast charge-discharge capacity, long cycle life and inherent biocompatibility. As a result, they have emerged as a strong candidate for satisfying the requirements of portable electronics [5,6]. Furthermore, electrode materials are crucial to the performance of paper-based supercapacitors. Therefore, the exploration and development of low-cost and high-performance paper-based electrode materials are the keys to the scalable applications of paper-based supercapacitors.

As the main component of papermaking pulp, cellulose fibers are inexpensive, renewable and biocompatible, making them the preferred raw material for green and sustainable energy storage applications [7–10]. However, cellulose is an insulator, which prevents itself from direct applications in storing electrical energy. Common strategies for

elevating electrical conductivity and facilitating energy storage in paper are to deposit [11,12], impregnate [13], filter [14,15], coat [16,17], or mix [18,19] conductive and electroactive substances (e.g., graphene, carbon nanotubes, polyaniline, polypyrrole, etc.) with cellulose fibers. For instance, carbon nanotubes (CNT) ink was coated on a commercial printing paper to prepare a paper-based electrode with a specific capacitance of 200F/g (based on the mass of CNT alone). Moreover, the CNT ink significantly improved its adhesion to the paper substrate and mechanical properties of the coated paper compared with polyethylene terephthalate (PET)[16]. To further improve CNT adhesion on paper substrates, Li et al.[20] designed a hybrid paper incorporating bacterial cellulose into the cellulose fiber matrix, which possessed extraordinary cycling stability and specific capacitance of 16.3F/cm³ (or 77.5F/g). Nevertheless, the need for expensive electroactive substances increases the cost, and the non-conductive cellulose fiber matrix restricts the further improvement of specific capacitance of the entire paper-based electrode. More recently, loading active substances on single nanofibers were found to improve the overall gravimetric and volumetric

* Corresponding author.

E-mail address: felhl@scut.edu.cn (H. Li).

performance of electrodes [21,22]. However, this method suffers from the complexity of the loading operation, making it undesirable for mass production. On the other hand, cellulose has been used as a precursor to prepare conductive, cellulose-derived carbon by carbonization or activation [23–25]. This process can retain the morphology, porous structure and self-supporting nature of papers, resulting in the improved capacitance of electrodes [26]. However, some problems of the prepared cellulose-derived carbon papers can be summarized that the apparent loss of mechanical flexibility and the limitation of the subsequent processability. Given the deficiencies in current paper electrode performance and preparation methods, developing low-cost, high-performance paper-based flexible electrode materials with a process suitable for mass production remains a challenge and a vital research topic.

Carbon fibers (CFs) have been widely used to reinforce composite materials due to their high strength and stiffness [27–29]. Moreover, CFs have lightweight, low thermal expansion coefficient, and high electric conductivity, which have been explored as electrode materials in flexible supercapacitors [30–32]. However, the low specific surface area (SSA) ($<10 \text{ m}^2/\text{g}$) and poor porosity of CFs resulted in unsatisfactory capacitive performance. To mitigate this problem, high SSA carbon materials [33,34] and pseudocapacitive materials [35] were introduced, and CFs were activated to increase their electroactivity and SSA [32,36]. Activated carbon fibers (ACFs) had high SSA and exposed micropores on the fiber surface, facilitating rapid ion absorption and desorption during charging and discharging processes [37,38]. Commercial ACFs are mostly spun from petrochemical products (polyacrylonitrile, phenolic resin, asphalt) into fibers and subsequently carbonized and activated, increasing the dependence on petroleum resources. While the use of pulp fibers, prominently cellulose, to prepare ACFs are conducive to the sustainable utilization of resources and the reduction of cost due to the abundant, inexpensive and renewable of plant resources. In addition, pulp fibers are easily fibrillated, resulting in a hairy surface by beating process [39,40]. The same process could increase the SSA of pulp fibers and interweaving of fibers, thereby improving papers' strength and flexibility.

Herein, a facile and economical strategy is proposed to fabricate low-cost, high-performance cellulose-based activated carbon fiber papers (ACFPs) with high electrical conductivity, electrochemical performance, and mechanical flexibility. The material costs and preparation methods of this work and previous report were also compared in Table S1 (Supporting information), which indicated the ACFPs electrode was competitive. The strategy combines composite papermaking and the continuous thermal carbonization, double activation ($\text{H}_3\text{PO}_4 + \text{CO}_2$) process. First, fibrillated pulp fibers and CFs are mixed to form primary composite papers (CPs) with high mechanical strength and electrical conductivity. The CPs are then impregnated with phosphoric acid (H_3PO_4) solution. In the subsequent pyrolysis, CFs serve as the framework in ACFPs due to their low thermal expansion coefficient and high chemical stability. At the same time, fibrillated pulp fibers are transformed into activated carbon fibers (ACFs) which provide capacitive energy storage sites in ACFPs. H_3PO_4 in CPs promotes cellulose hydrolysis, enhancing the adhesion between ACFs matrix and CFs and providing active sites for subsequent double activation. Overall, this work tests the effectiveness of the new strategy to achieve high-performance paper-based electrode materials and shows broad application prospects in the field of energy storage.

2. Experimental

2.1. Materials

Cotton pulp board; 3 mm CFs (Japan Toho Chemical Industry Co., Ltd., T series); H_3PO_4 (H_3PO_4 purity $\geq 85\%$); High-purity nitrogen (N_2 purity $\geq 99.999\%$); Food-grade carbon dioxide gas (CO_2 purity $\geq 99.9\%$). All the above reagents and raw materials are from commercial

products.

2.2. Preparation of the primary CPs

Preparation of fibrillated cotton pulp: the cotton pulp board was placed in Walli Beater (PL4-2, Xianyang Test Equipment Co., Ltd.) with 1 wt% concentration for 10 min, and then 5.5 kg was loaded for beating 15 min. Next, the cotton pulp fibers were drained out and balanced the moisture to calculate its dryness. Finally, PFI mill (Mark V1, HAMJERN MASKIN 621, Norway) was used to refine the pulp fibers with 10 wt% pulp consistency until the beating degree of fibers were 40°SR.

Preparation of primary CPs: fibrillated pulp fibers and CFs with a certain absolute dry mass ratio were placed in a deflaker with water, then put it in Automatic Sheet Shaper (NO 2542-A, Kumagai Riki Kogyo co., Ltd) to form the paper and dried in Flat Pattern Dryer (PL7-C, Xianyang Test Equipment Co., Ltd.) to obtain primary CPs. All Primary CPs were prepared with the same grammage of $80 \text{ g}/\text{m}^2$ and labeled as xx% CF (xx was the addition amount of CFs).

2.3. Preparation of the cellulose-based ACFPs

Primary CP with xx% CF in section 2.2 was pre-impregnated with a mass impregnation ratio of 1.5:1 (H_3PO_4 to paper) in 20% H_3PO_4 solution for 14 h. The impregnated paper was placed in a tube furnace, then carbonized and activated at 450°C in N_2 atmosphere for 1 h. When the temperature was heated to 850°C , the sample was continued to activate under CO_2 atmosphere for 1 h. Afterwards, the sample was taken out when it cooled to room temperature. Finally, it was repeatedly washed with deionized water to neutral and dried to obtain cellulose-based ACFP and labeled as ACFP-xx.

2.4. Fabrication of the all-solid-state supercapacitors based on ACFP-15

The all-solid-state symmetric supercapacitor (SSC) was fabricated using two pieces of ACFP-15 as electrodes ($1.4 \times 4 \text{ cm}$), a cellulose paper as separator (1.5×2.2), and PVA-KOH gel as solid electrolyte. The PVA-KOH gel was obtained as follows. Firstly, 1.5 g KOH was dissolved in 5 mL distilled water. Secondly, the PVA (3 g) was added distilled water (25 mL) and stirred for 4 h at 90°C . Then the PVA-KOH gel was obtained by mixing above solution and stirring for 3 h at 60°C . For fabricating the all-solid-state SSC, ACFP-15 were partially immersed (1.4×2.2) into the PVA-KOH gel and placed in the vacuum drying oven (room temperature) to ensure that the electrolyte is fully immersed in the electrode. Subsequently, cellulose separator was put onto middle of two pieces of the resulting ACFPs covered by the gel electrolyte. The middle part was wrapped with PET film, the portion of the electrode not impregnated with electrolyte is exposed. After that, the SSC was dried in room temperature to remove excess water.

2.5. Preparation of manganese dioxide (MnO_2)-ACFP

The MnO_2 electrodeposition was performed on ACFP ($1 \times 1 \text{ cm}^2$) at $1 \text{ mA}/\text{cm}^2$ in 0.1 M manganese sulfate solution at room temperature, using Ag/AgCl and Pt foils as reference and counter electrodes, respectively. After 3 h of deposition, the sample were washed with deionized water and vacuum dried at 60°C to obtain MnO_2 -ACFP.

2.6. Materials characterizations

The microscopic morphology of the samples was characterized by field emission scanning electron microscope (FE-SEM, Merline, Zeiss). The SSA (ASAP 2460, Micromeritics) was used to characterize and analyze the specific surface area (calculated by the BET method) and the pore size distribution (DFT model) of the sample using N_2 adsorption. X-ray diffractometer (XRD, X'pert Powder, PANalytical) and Raman microscope (Raman, LabRAM Aramis, Horiba Jobin Yvon) were used to

analyze the phase and structure changes of the samples. Fourier transform infrared spectroscopy (FTIR, vertex70, bruker) was used to confirm changes of functional groups of the samples. Four probes (RTS-8, Guangzhou Four Probe Technology Co., Ltd.) can be used to test the square resistance and conductivity of the samples. A material testing machine (INSTRON 3300, USA) was used to measure the tensile properties of ACFPs according to the national standard GB/T2004.7–2014. In detail, the materials were cut into rectangular shapes of 70 mm × 15 mm, and the tensile speed was 10 mm/min.

2.7. Electrochemical performance characterization

The electrochemical workstation (CHI660E, Shanghai Chenhua Instrument Co., Ltd.) was used to test the cellulose-based ACFPs electrochemical properties with a three-electrode test system (Pt, Hg/HgO, 1 × 1 cm² of ACFPs) in 6 M KOH electrolyte. In addition, the electrochemical performance of MnO₂-ACFP was carried out by three-electrode test system (Pt, Ag/AgCl, 1 × 1 cm of MnO₂-ACFP) in 1 M Na₂SO₄ electrolyte. The electrochemical performances of samples were researched by cyclic voltammetry (CV), galvanostatic charge/discharge (GCD), electrochemical impedance spectroscopy (EIS, 10⁶ to 10–2 Hz, 10 mV amplitude) and cycle testing. The detailed calculation process of electrodes specific capacitance refers to [supporting information](#).

3. Results and discussion

3.1. Design principle and fabrication of cellulose-based ACFPs

Fig. 1a displays the schematic illustration of the fabrication of cellulose-based ACFPs. Fibrillated pulp fibers and CFs were mixed in a certain proportion to fabricate primary CPs through the papermaking process. Then the ACFPs were prepared by pre-impregnation of 20% H₃PO₄ solution, and the continuous thermal carbonization, double activation (H₃PO₄ + CO₂) process. The surface of the CFs has grooves and uniform diameters with 7 μm (**Fig. 1b** and **Fig. S1, Supporting Information**). While more fibrillated pulp fibers were obtained by beating cotton pulp, which can expose more fine fibers to increase SSA (**Fig. 1c** and **Fig. S2**) and easily intertwine CFs to generate a fibrous network. Except for the interweaving of fibers, the partial hydrolysis of fibrillated pulp fibers can produce oligosaccharides and monosaccharides due to pre-impregnation of H₃PO₄ solution (**Fig. 1d**), which can cross-linked with H₃PO₄ to form phosphate ester bonds [41,42]. This process can contribute fibers to stick together before completely converted to ACFs matrix. Meanwhile, the CFs were tightly wrapped in it during subsequent carbonization and activation process to increase the strength of ACFPs (**Fig. 2d-f**). Due to the low thermal expansion coefficient and high chemical stability of CFs, it can also serve as a framework for ACFPs. Consequently, the prepared ACFP have flexible mechanical properties which can be folded, rolled (**Fig. 1e**). Moreover, it also can be directly used as self-supporting electrodes. When the LED lamp touched with the ACFP, it can light up stably (**Fig. 1f**), demonstrating ACFP has excellent electrical conductivity. The composite three-dimensional network structure offers good channels for the transmission of electrons and the storage of ions. As proved in below discussion, this work provides an economical and simple method for the preparation of cellulose-based ACFPs, realizing the integration of high performance and processable electrode materials.

H₃PO₄ solution, and the continuous thermal carbonization, double activation (H₃PO₄ + CO₂) process. The surface of the CFs has grooves and uniform diameters with 7 μm (**Fig. 1b** and **Fig. S1, Supporting Information**). While more fibrillated pulp fibers were obtained by beating cotton pulp, which can expose more fine fibers to increase SSA (**Fig. 1c** and **Fig. S2**) and easily intertwine CFs to generate a fibrous network. Except for the interweaving of fibers, the partial hydrolysis of fibrillated pulp fibers can produce oligosaccharides and monosaccharides due to pre-impregnation of H₃PO₄ solution (**Fig. 1d**), which can cross-linked with H₃PO₄ to form phosphate ester bonds [41,42]. This process can contribute fibers to stick together before completely converted to ACFs matrix. Meanwhile, the CFs were tightly wrapped in it during subsequent carbonization and activation process to increase the strength of ACFPs (**Fig. 2d-f**). Due to the low thermal expansion coefficient and high chemical stability of CFs, it can also serve as a framework for ACFPs. Consequently, the prepared ACFP have flexible mechanical properties which can be folded, rolled (**Fig. 1e**). Moreover, it also can be directly used as self-supporting electrodes. When the LED lamp touched with the ACFP, it can light up stably (**Fig. 1f**), demonstrating ACFP has excellent electrical conductivity. The composite three-dimensional network structure offers good channels for the transmission of electrons and the storage of ions. As proved in below discussion, this work provides an economical and simple method for the preparation of cellulose-based ACFPs, realizing the integration of high performance and processable electrode materials.

3.2. Characterization of cellulose-based ACFPs morphology and structure

The primary CPs with same grammage was prepared by mixing fibrillated pulp fibers and CFs in a certain proportion. Taking primary CP with 15% CF content for example (**Fig. 2a-c**), CFs were uniformly dispersed in the paper (yellow arrows position in **Fig. 2a**), and fibrillated

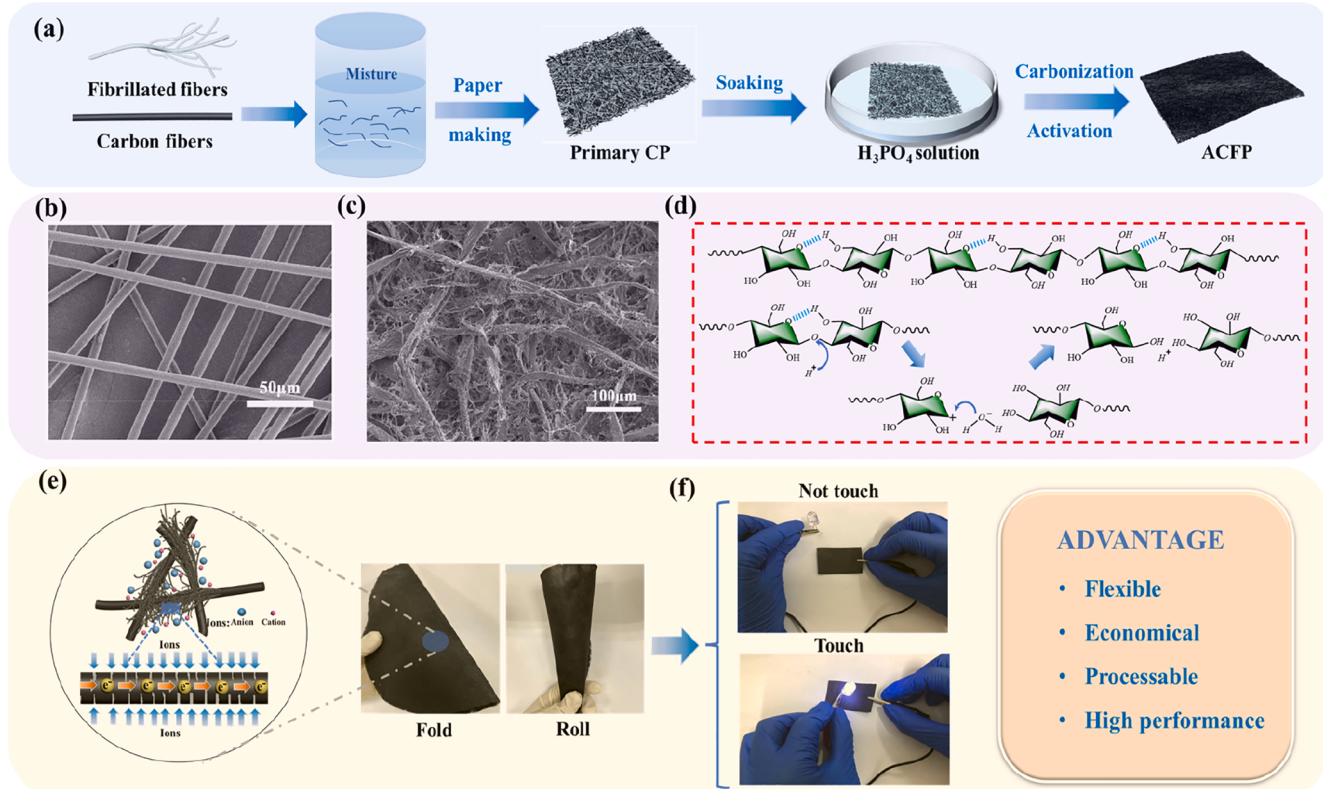


Fig. 1. (a) Schematic illustration of the fabrication of cellulose-based ACFPs. (b) SEM images of CFs. (c) SEM images of fibrillated pulp fibers. (d) Schematic illustration of the partial hydrolysis of fibrillated fibers after H₃PO₄ impregnation (e) Digital photo of ACFP and mechanism of ion and electron transport of ACFP as a self-supporting electrode. (f) Circuit experiment of ACFP and its advantages in application.

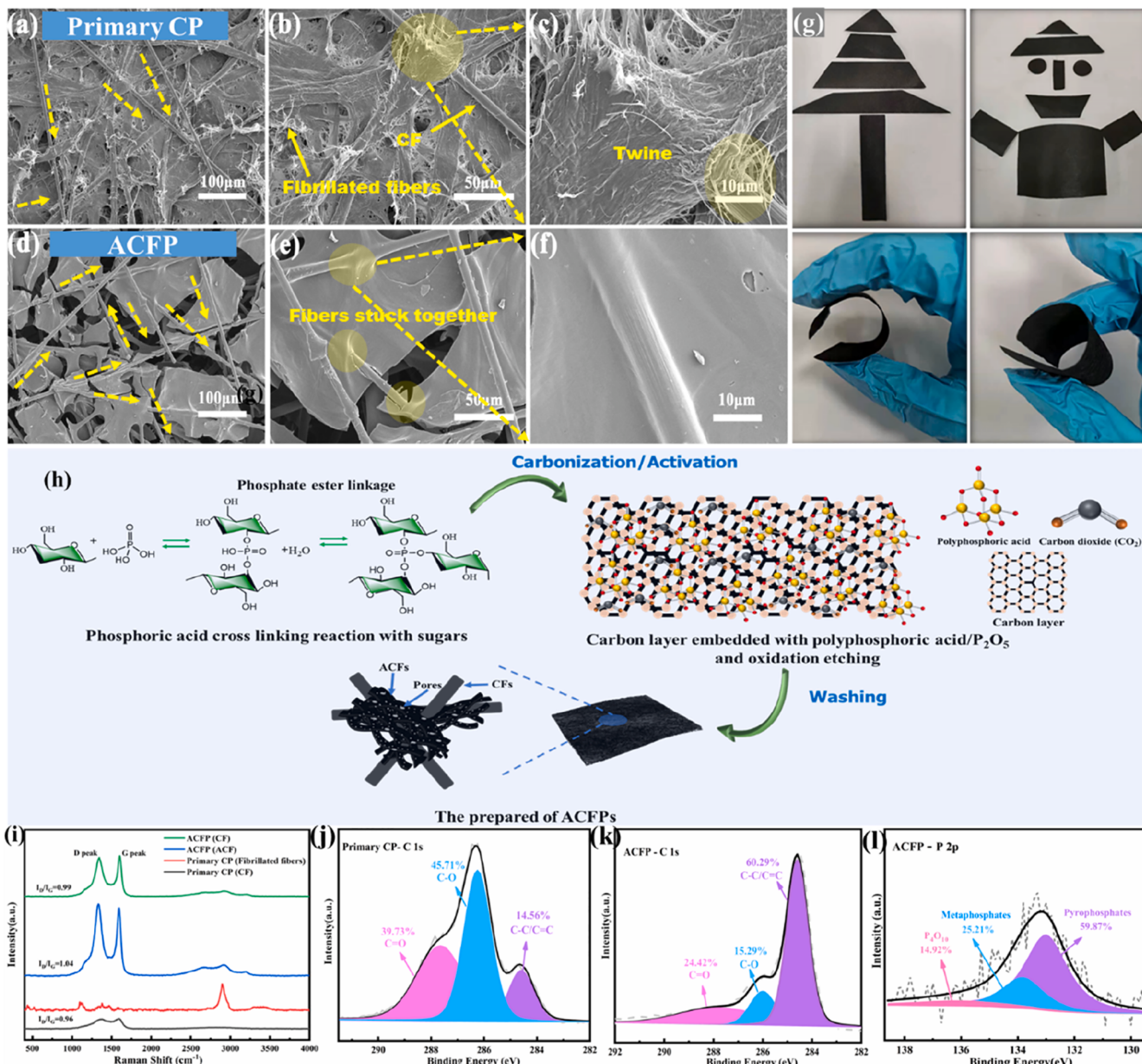


Fig. 2. (a–c) SEM images of primary CP (15% CF content) with different magnification. (d–f) SEM images of cellulose-based ACFP-15 with different magnification. (g) Photographs of cellulose-based ACFP-15. (h) The process and mechanism of ACFP structure and pore formation. (i) Raman spectra of primary CP (15% CF content) and cellulose-based ACFP-15. (j–k) High-resolution XPS C1s spectra of primary CP (15% CF content) and cellulose-based ACFP. (l) High-resolution XPS P2p spectra of cellulose-based ACFP.

pulp fibers were tightly twined on the CFs (Fig. 2b–c), which was facilitated to form a compact structure of paper. Subsequently, the primary CP was pre-impregnated with H_3PO_4 solution, thermal carbonized and double activated ($H_3PO_4 + CO_2$) to prepare cellulose-based ACFPs. Fig. 2d–f exhibited SEM images of cellulose-based ACFP-15. It was clear that ACFP-15 presented more gaps than the compact primary CP due to the thermal shrinkage of pulp fibers at high temperatures (Fig. 2d–e). Nevertheless, the morphology of CFs had no obvious change in this process, which were related to its low thermal expansion coefficient and good thermal stability. Thus, CFs can serve as the conductive skeleton of ACFPs to ensure the integrity and the superior conductive of paper. Meanwhile, fibrillated pulp fibers can be converted into ACFs matrix to increase its pore structure, which was proved in TEM images (Fig. S3a–c). It can be observed that ACFs matrix was a typical amorphous carbon structure, which had disordered network with coiled and twisted streaks, accompanying by local parallel arrangements of sporadic

fragments. The disordered mesopore and micropore structures also can be seen in the lightness and darkness of the image [43], thereby providing channels for ion transport. In addition, it should be noticed that the matrix surface of the ACFs was relatively smooth (Fig. 2e–f), rather than the original “fuzz” (Fig. 2b–c). Moreover, traces of fibers lapped on the CFs can be observed (yellow circles in Fig. 2e), and it seemed CF was embedded in the ACF matrix (Fig. 2f). The possible reason behind this phenomenon and the formation mechanism of pores in ACFPs can be explained as shown in Fig. 2h. Pulp fibers could produce oligosaccharides and glucose when it was partially hydrolyzed under H_3PO_4 pre-impregnation. With the increase of temperature, the flow of oligosaccharides intensified, which also promoted its cross-linking with H_3PO_4 to form phosphate ester bonds. Meanwhile, the fibers “glued” together, and the CFs were also wrapped in it. After pyrolysis, the carbon layer containing polyphosphoric acid or phosphorus oxide (P_4O_{10}) was formed. Due to the oxidation of CO_2 and P_4O_{10} , it can directly react with

the carbon layer to generate pores. Finally, excess polyphosphoric acid or phosphorus oxides were washed with distilled water to obtain pore-rich ACFPs. In addition, the FTIR was used to confirm the changes of functional groups in this process, the detailed description was displayed in the supporting information (Fig. S4).

To further illustrate design principles of cellulose-based ACFPs, it can be compared and demonstrated by ACFP prepared without CF addition and without immersing H_3PO_4 solution, respectively. The SEM images of ACFP prepared without CF addition was shown in Fig. S5a, the fibers were tightly bonded together and displayed a smooth surface. However, the paper structure was prone to break during the conversion to derived carbon, owing to the thermal shrinkage of cellulose and the absence of stable skeleton material connections. Therefore, it can be seen the photograph of ACFP became brittle paper pieces (Fig. S5b). Similarly, Fig. S5c exhibited SEM images of ACFP prepared without immersing H_3PO_4 solution. It was observed that the morphology of the fibers in ACFs were very obvious. But the interlacing between fibers decreased, and the gap increased due to the shrinkage during pyrolysis. ACFP can keep complete paper structure in this case (Fig. S5d), but it showed a poor strength and the tensile test cannot be carried out due to the lack of adhesion between fibers and the reduction of inter-fiber interlacing. While ACFP-15 prepared by CF addition and pre-impregnation with H_3PO_4 solution possessed flexible mechanical properties similar to normal paper. As shown in the Fig. 2g and Movie S1, the ACFP-15 could be cut, bent, and had high tensile strength (More details were discussed below in mechanical properties). Moreover, the ACFP-15 can withstand a pressure of 0.5 MPa (Fig. S6) and can also be manually folded more than 100 times (Movie S2). All in all, the synergistic effect of CF introduction and pre-impregnation of H_3PO_4 solution could enhance the strength of ACFPs, which provided premise guarantee for subsequent ACFPs to be directly used as self-supporting electrode.

Correspondingly, the structure of primary CP (15% CF content) and ACFP-15 was further characterized. Fig. S7 showed the XRD pattern of primary CP (15% CF content) and ACFP-15. The primary CP appeared representative diffraction peaks of (101), (10 $\bar{1}$) and (002) at 14.8°, 16.5°, and 22.6°, respectively, which were characteristic of cellulose I [44,45]. While the ACFP diffraction peak of type cellulose I disappeared and the wide diffraction peak of about 25° was obvious. This was related to the typical amorphous carbon structure in ACF [46]. The cellulose peaks at 1098 cm⁻¹ and 2895 cm⁻¹ in Raman spectrum [47] of primary CP (fibrillated fibers) were also disappeared after pyrolysis (Fig. 2i), which was consistent with XRD results. While two obvious absorption peaks (D peak, 1350 cm⁻¹; G peak, 1575 cm⁻¹) appeared in the obtained ACFP (ACF), representing the ordered and disordered structures in the carbon materials, respectively [48], It is indicated that ACFP (ACF) is an amorphous carbon structure containing graphitic crystallites, which also consistent with the reported results [49,50]. Moreover, the increasing value of I_D/I_G indirectly reflect the increase of disorder degree in CF structure during the activation process.

The surface elements and chemical valence states of primary CP (15% CF) and ACFP-15 were determined and analyzed by XPS (Fig. 2j-l, Table S2). The conversion of the fibrillated pulp fibers into ACFs resulted in decreases of C/O mass ratio, C/O single and C/O double bonds, which were consistent with expectations. A small amount of P element existed in ACFP, relating to the pre-impregnation of H_3PO_4 solution before pyrolysis. In the high-resolution spectrum of 2P of ACFP, the binding energies of P in three forms were 132.8 eV, 134.0 eV and 136.0 eV, respectively. These peaks can be assigned to pyrophosphate, metaphosphate and phosphorus pentoxide (P_4O_{10}), respectively [51,52]. This existence of phosphorus-containing functional groups was the result of crosslinking between phosphoric acid, the precursor of biomass, and carbon-containing fragments during the process of bond cracking reaction and activation [41,52].

3.3. Effect of CFs addition on the preparation of cellulose-based ACFPs

Commercial carbon paper is mainly made of CFs, which has low SSA (<10 m²/g) and low specific capacity [21,41]. As for ACFPs, the cellulose-based ACF matrix provides it a larger SSA, while its conductivity mainly depends on the addition of CFs. Therefore, for the same grammage of primary CPs, the content of CFs has a considerable influence on the performance of prepared ACFPs. Considering the heat loss of pyrolysis process, the addition of CFs in primary CPs are limited to <45% to ensure that the prepared ACFPs have good energy storage effect. Fig. 3a showed the digital and SEM images of the primary CPs with different CFs content under the same grammage condition. It can be obviously observed that with the increase of CFs addition, the color of primary CPs gradually became darker, the interlacing between fibrillated fibers decreased. The SEM figures of ACFPs obtained by primary CPs with different CFs addition after pyrolysis were shown in Fig. 3b. The CF was also tightly embedded in the ACFs matrix, which had been discussed in 3.2 (Fig. 2d-f). In addition, the yield of ACFPs also increased with the initial CFs addition (Table S4), which indirectly reflected the stability of CFs before and after pyrolysis. Nevertheless, due to the heat loss of cellulose during pyrolysis, the higher initial addition of CFs under the same grammage of primary CPs, the lower content of ACFs in the prepared ACFPs. Thus, it can be noticed in Fig. 3b that stickiness between CFs and ACFs decreased, and the larger gap in paper appeared with the increase of CFs, which may inevitably lead to the decline of paper strength. Therefore, the optimal addition of CFs and the detailed effects of the prepared ACFPs performance need to be determined in further research.

It has been demonstrated that ACFP-15 has flexible mechanical property in section 3.2. Furthermore, the tensile property of prepared ACFPs with different CFs addition were also explored, as shown in Fig. 4a. Thereinto, the ACFP cannot be formed a complete paper structure when the initial CFs content were <2%. Moreover, with the increase of the CFs addition, the strength of the prepared ACFPs increased continuously until the tensile strength of ACFP-15 reached the maximum of 6.4 MPa and Young's modulus reached 1185 MPa. While CFs addition exceeded 15%, the tensile property of ACFPs gradually decreased due to the corresponding decline of stickiness between ACFs and CFs, which was consistent with the results envisaged by the SEM analysis (Fig. 3b). Noticeably, the maximum tensile property of ACFP can be regarded as strong paper in comparison with graphene paper (5.13 MPa) [14], cellulose/RGO paper (1.2 MPa) [53], and cellulose/CNT paper (1 MPa) [54]. In order to clearly comprehend the tensile fracture mechanism of ACFPs, further microscopic and SEM observations were conducted on the fracture after tensile test. At the yellow arrow in Fig. 4b, the groove left after the CF was pulled out can be clearly observed. Thus, it can be evidently demonstrated that the tensile fracture of ACFP is mainly caused by the pullout of CF from the ACF matrix and the break of the ACF matrix.

According to the formula: $R = \rho/t$, square resistance (R) is inversely proportional to the thickness (t) and directly proportional to the resistivity (ρ) [55]. In detail, the thickness, square resistance and conductivity of primary CPs and ACFPs prepared with different CFs addition were listed in Tables S3 and S4. With the raising of CFs addition, the increase of thickness and the inverse decrease of square resistance for primary CPs can be observed. Moreover, the electrical conductivity of ACFPs were greatly increased, and the thickness decreased after pyrolysis, mainly due to the transformed ACFs from pulp fibers. Fig. 5c showed the square resistance and electrical conductivity of ACFPs with different initial CFs content. The electrical conductivity of ACFPs increased first and then decreased with the increase of relative CFs content, which reached a maximum of 1786 S/m in ACFP-15. While the decrease of square resistance from 14.3 Ω/sq to 3.1 Ω/sq can be attributed to the changes of relative content of CFs. Moreover, the conductivity and square resistance of ACFPs show greater superiority compared with the cellulose-based conductive papers that have been

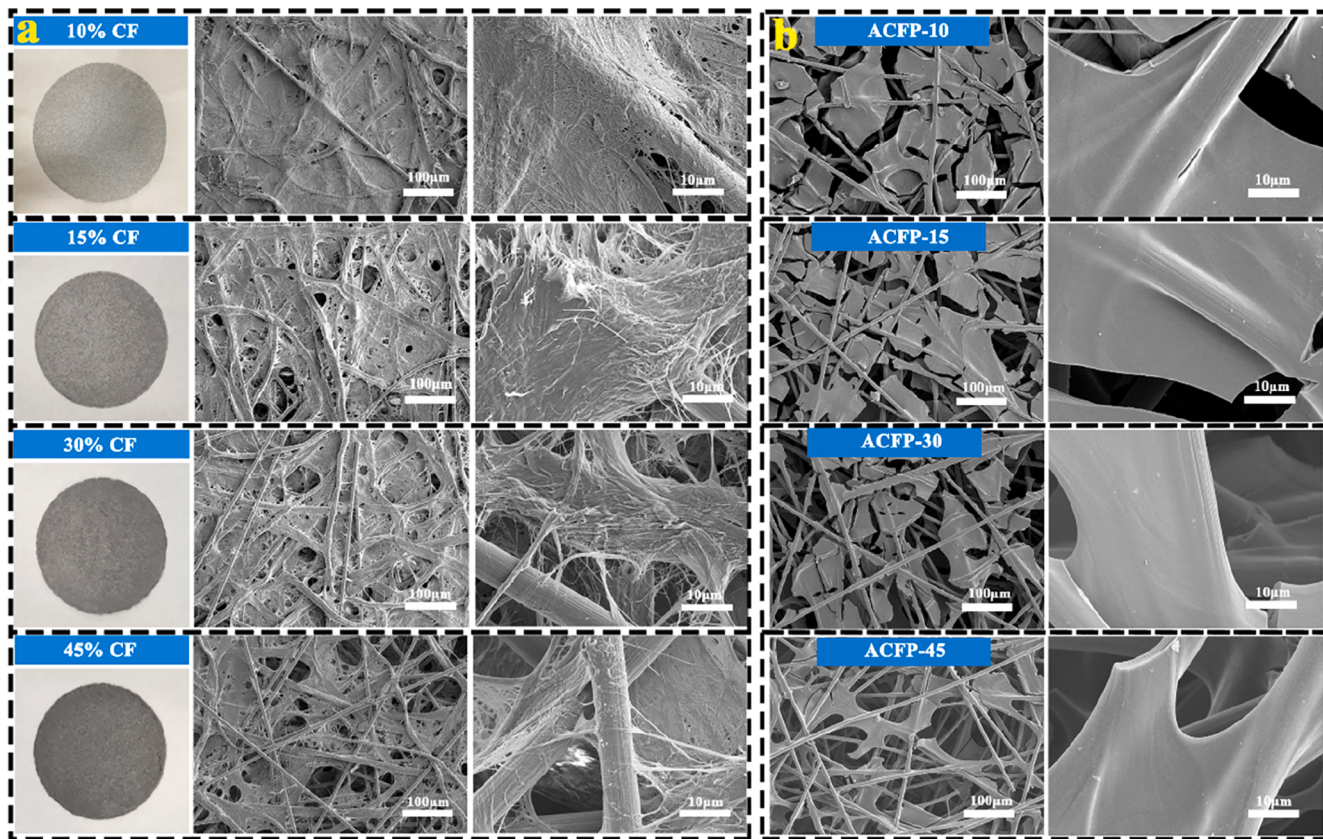


Fig. 3. (a) Photographs and SEM images of primary CPs with different magnification (10% CF, 15% CF, 30% CF, 45% CF). (b) SEM images of cellulose-based ACFPs with different magnification (ACFP-10, ACFP-15%, ACFP-30, ACFP-45).

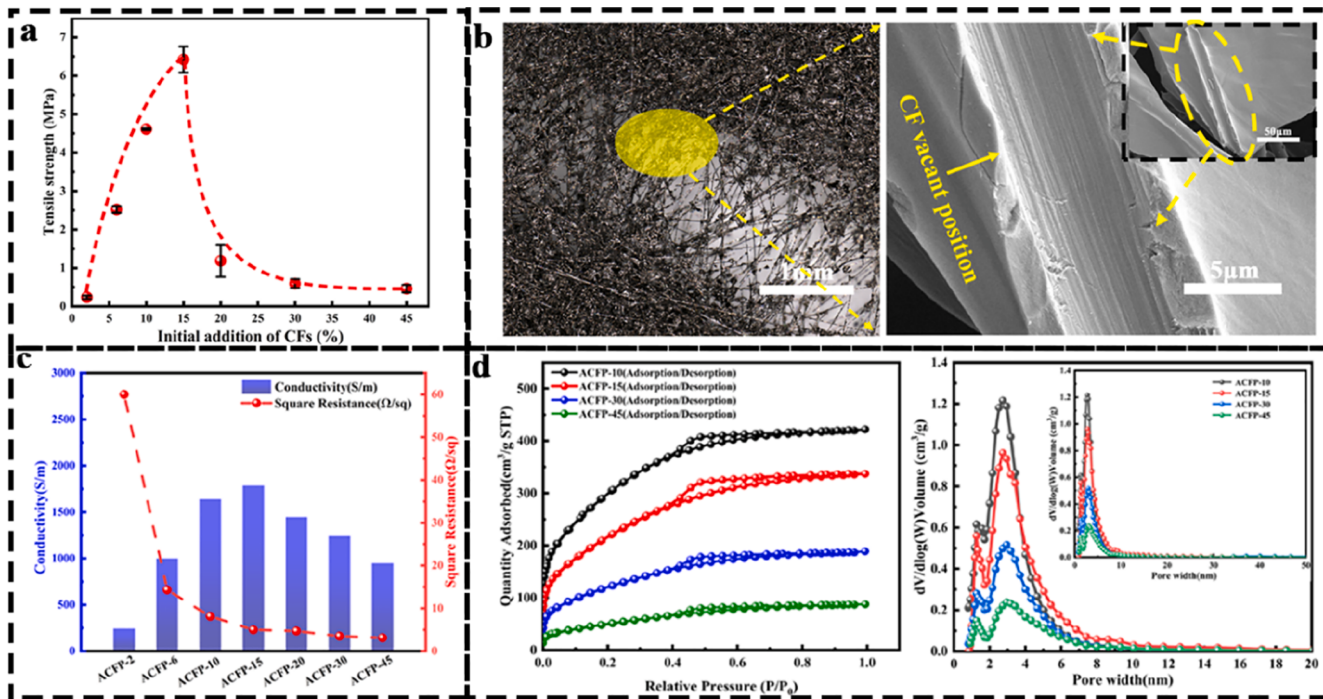


Fig. 4. (a) Tensile strength of cellulose-based ACFPs with different CFs content. (b) Microscope image and SEM image of the ACFP fracture. (c) Square resistance and electrical conductivity of cellulose-based ACFPs with different CFs content. (d) N₂ adsorption isotherms and pore size distributions of ACFPs with different CFs content.

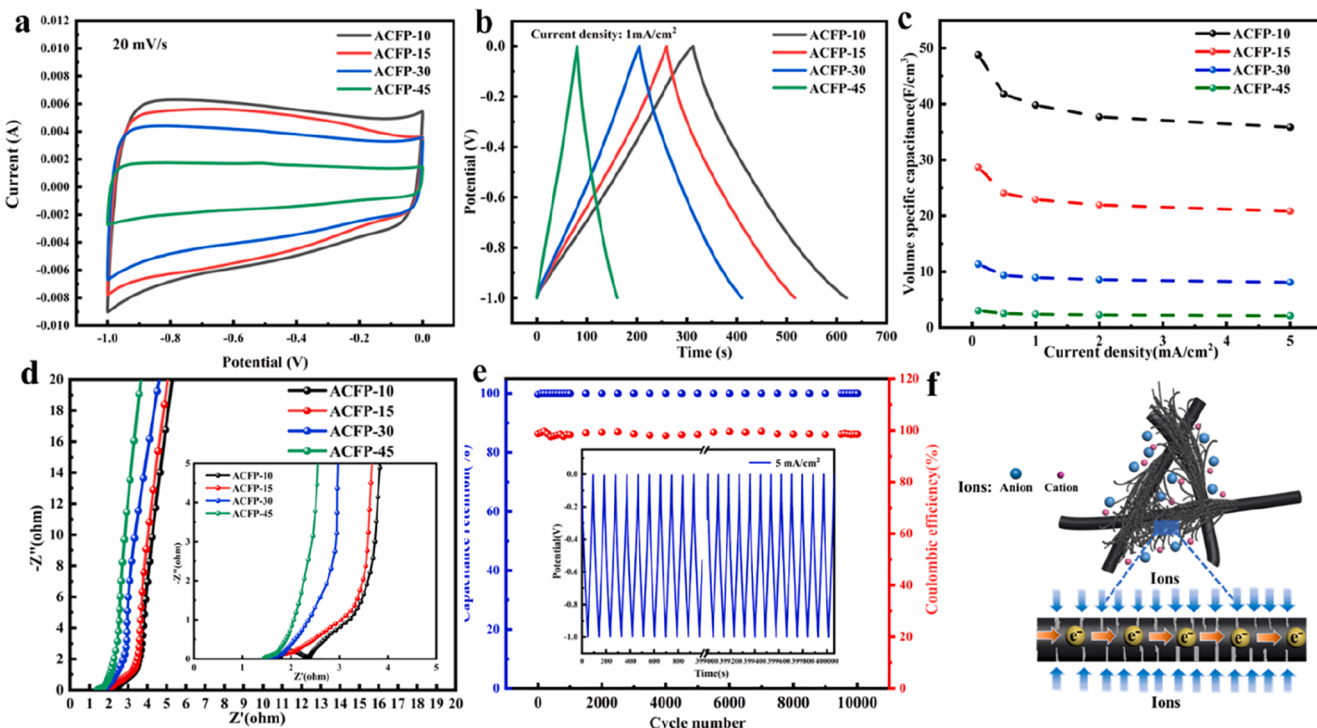


Fig. 5. (a) Cyclic voltammetry (CV) curves of ACFPs with different CFs content at 20 mV/s scan rates. (b) Galvanostatic charge and discharge (GCD) curves of ACFPs at 1 mA/cm² current densities. (c) Volume specific capacitance of ACFPs at different current densities. (d) Electrochemical impedance spectra of ACFPs with different CFs content. (e) Capacitance retention and coulombic efficiency at a current density of 5 mA/cm². Inset: 10,000 cycles of GCD curve. (f) Schematic diagram of charge transfer and electrolyte ion transfer in conductive networks in ACFP.

reported (Table S5).

In addition, the gas adsorption method was used to further demonstrate the pore structure of ACFPs. The SSA and pore size distribution of ACFPs with different relative CFs content were shown in Fig. 4d. The adsorption capacity of N₂ increased rapidly at low pressure stage, revealing a certain microporous structure due to the strong force between adsorbent and adsorbate. As the relative pressure continued to increase, a hysteresis loop appeared in the adsorption isotherm because of capillary condensation of N₂, which demonstrated that the sample had a mesoporous structure. The adsorption capacity of ACFP-10 was significantly higher than that of other samples, indicating that it had the largest SSA (1106 m²/g). The SSA was much higher than the reported electrode materials (Table S6), which was favorable for ion storage. From pore size distribution and three-dimensional structure of ACFPs, typical porous carbon structures in ACFPs, including micropores (<2 nm), mesoporous pores (2–50 nm) and macropore (>50 nm), were favorable for the diffusion and storage of ions. The detailed SSA values and pore structure parameters were shown in Table 1. With the increase of CF addition, the SSA as well as micropore ratio of the prepared ACFPs gradually decreased. This result supported the conclusion that the micropores and SSA are mainly derived from ACFs matrix.

3.4. Electrochemical properties of ACFPs as self-supporting supercapacitor electrodes

ACFPs were directly used as electrodes without any binder, and the electrochemical performance in a three-electrode system was researched. Fig. 5a showed CV curves of ACFPs with different CFs contents at 20 mV/s. These rectangular CV curves indicated ACFPs had an excellent electric double layer capacitive behavior. The quasi-rectangular shapes of the CV curves were generally remained, even at a high scanning speed of 200 mV/s, demonstrating the fast current response on voltage reversal and low resistance of ion transport (Fig. S8). Typical GCD curves at current density of 1 mA/cm² were plotted in Fig. 5b, the nearly linear GCD curves with a triangular and symmetric shape were implications of a high coulombic efficiency. Moreover, the gradually increased discharge time and rectangular area from ACFP-45 to ACFP-10, suggesting the substantially increases of charge-storage capability. Specifically, GCD curves of ACFPs were tested under various current densities (Fig. S9), so the specific capacitance can be calculated, based on the overall volume, mass, and area of ACFPs, respectively (Fig. 5c, Fig. S10). Among them, ACFP-10 displayed highest specific capacitance due to the largest SSA, the volume specific capacitance and mass specific capacitance at 0.1–5 mA/cm² of ACFP-10 were 35.8–48.8 F/cm³, 121–165 F/g, respectively. In addition, ACFP-15 with excellent mechanical properties can also reach 20.8–28.7 F/cm³ (76–105 F/g). However, the maximum specific capacitance of ACFP-45 was reduced to 3 F/cm³ (23 F/g), which confirmed that ACFs were the main sites for ACFPs ion energy storage.

In order to further evaluate the impedance and ion transfer behavior of ACFPs with different CFs contents, EIS was measured as shown in Fig. 5d. As the CFs content increased, the x-intercept in the high-frequency region of the Nyquist plot gradually decreased, indicating that the equivalent series resistance reduced. Meanwhile, the gradually vertical lines in low-frequency region indicated its nearly ideal capacitive behavior [56]. Especially for ACFP-45, it exhibited a nearly straight

Table 1
Specific surface area and pore structure parameters of ACFPs.

Sample	S _{BET} (m ² /g)	V _{tot} (cm ³ /g)	V _{mi} /V _{tot} (%)	D (nm)
ACFP-10	1106	0.65	51.4	2.35
ACFP-15	808	0.52	23.0	2.56
ACFP-30	450	0.29	20.0	2.56
ACFP-45	190	0.13	10.0	2.82

line and small semicircle, revealing an ideal capacitance performance and a small resistance to charge and mass transport. Moreover, the phase angle value in the Bode plots gradually tend to 90° with more CF addition, which was closer to the ideal double electrode layer capacitive behavior (Fig. S11a). To gain more insights into frequency response characteristics of ACFPs, Fig. S11b showed the evolution of virtual capacitance (C'') versus frequency. It was observed that C'' increased sharply with the decreasing frequency. When the peak was reached, it represented the transition from pure resistance to pure capacitance. The frequency at the maximum value of C'' corresponded to the double-layer relaxation time constant (τ) established by the capacitor (τ is the inverse of the frequency) [57]. The time constant of ACFPs were all within 10 s, which indicated the fast establishment of double layer. This result was much faster than reported in some literatures [58,59]. In addition, the ionic impedance R_i of ACFPs in electrolyte also decrease, which can be determined by the relationship between C'' and the impedance of the real part (Z'), as shown in Fig. S11c. The highly conductive electrode interface enhanced the attraction of electrolyte ions, thereby reducing the resistance to ion transport. In a word, the addition of CFs was beneficial to the conduction of electrons and the migration and diffusion of electrolyte ions in ACFPs, which can significantly improve the capacitive behavior and power characteristics of ACFPs.

Considering the energy storage, impedance, and mechanical properties of ACFPs, the ACFP-15 was selected for 10,000 cycles stability evaluations. The results in Fig. 5e showed the coulombic efficiency and the capacity retention remained to be 98.58% and 100% after 10,000 cycles, respectively, revealing a prominent long-term cycle stability. Based on the good energy storage effect and stability of ACFP, Fig. 5f interpreted the schematic diagram of charge transfer and electrolyte ion transfer in the paper network of ACFP as a self-supported electrode. A stable three-dimensional conductive network structure can be formed by CFs through tightly lapping in the ACF matrix, so that electrons can rapidly migrate along CF and also enhance the adsorption of electrolyte ions by ACFs. Meanwhile, the multi-pore structure of ACFP also provided a good channel for ion transport and storage.

Finally, we compared the cellulose-based ACFPs with the current research on similar electrode materials, as shown in Table 2. The specific capacitance of the ACFPs prepared in this study was superior to that of most carbon-based paper electrode materials, and was also comparable to that of pseudocapacitive paper-based materials. In terms of electrical conductivity and cycle stability, it was significantly better than many similar materials. Therefore, ACFPs prepared by this method has a good application prospect in the field of energy storage as an integrated electrode.

To further illustrate the performance of the ACFP electrodes as electrochemical energy storage, all-solid-state SSC were assembled

using the same two ACFP-15 electrodes with PVA-KOH gel electrolyte and a cellulose paper separator, as described in Fig. S12a. Fig. S12b displayed CV curves of all-solid-state SSC tested in a two-electrode system at different potential windows. It was observed the maximum potential window of the SSC can be chosen as 2.0 V. The CV curves (Fig. S12c) of the SSC device at various scan rates (20 to 500 mV/s) revealed similar shapes even at a high scan rate of 100 mV/s, which revealed a good capacitive behavior. According to the discharge curve of GCD curves (Fig. S12d), we calculated the mass specific capacitance (14.5–21.6 F/g) of ACFP-15 at different current densities (0.35–10 mA/cm²) to evaluate SSC device's energy and power density. More impressively, the SSC device delivered a high energy density of 6.01 Wh/kg at power density of 28.22 W/kg, and it maintained 4.03 Wh/kg at energy density and 806.45 W/kg at power density (Fig. S12e), which was better than some previous carbon-based electrode (Table S12f). In addition, in order to further evaluate its flexibility, the SSC was measured after it was folded. The results showed that folding the device had little effect on the CV curves, demonstrating an excellent flexibility.

3.5. Expansion research of ACFPs performance

From the above discussion, adding appropriate CFs (10–15%) in primary CPs can prepare ACFPs with high specific surface area (808–1106 m²/g), high conductivity (1640–1786 S/m), excellent tensile strength (4.6–6.4 MPa), and Young's modulus (1038–1185 MPa). Moreover, whether in an acidic, alkaline or neutral electrolyte, ACFPs can still maintain good wettability (Fig. S13a). After being placed in different electrolytes for more than 3 months, no powder was dropped from ACFP, and the electrode structure was intact (Movie S3). In addition, as illustrated in Fig. S13b, the contact angle of 66.5° for the ACFP-15 can be observed, also revealing the good wettability of ACFPs. Meanwhile, there was no obvious change in the CV curves before and after soaking for 3 months in KOH electrolyte (Fig. S13c), indicating ACFPs also possessed considerable durability and structural stability.

In addition, pseudocapacitive materials can be loaded in the three-dimensional structure of ACFPs, which further improves its energy storage effect. Taking loaded MnO₂ as an example, the loading capacity on ACFP-15 reached 5.3 mg/cm² after 3 h electrochemical deposition. Fig. S14 showed the SEM image of ACFP-15 after electrochemical deposition of MnO₂ and elemental mapping images of O, C and Mn, respectively. Due to the good electrical conductivity of ACFP, MnO₂ was uniformly loaded on CF and ACF matrix. Then, the electrochemical performance of the ACFP-15-MnO₂ was tested in 1 M Na₂SO₄ electrolyte, and its CV curve and GCD curve were shown in Fig. S15a and Fig. S15b. Based on the calculation of the entire electrode, the volume specific capacitance was 68 F/cm³ (corresponding area specific

Table 2
Comparison of carbon-based paper electrode materials prepared by different methods.

Materials	Capacitance (F/cm ³)	Capacitance (F/g)	Cycle stability	Conductivity (S/m)	Reference
Bacterial cellulose /CNT	–	74 ^a	99.5% after 1000 cycling (polyaniline addition)	–	[60]
Cellulosic fiber/CNT	16.3 ^b	77.5 ^a	98.4% after 15,000 cycling	590	[20]
Cellulose /reduced graphene oxide (RGO)	2.4 ^b	212 (based on RGO mass, 0.5 A/g)	94% after 14,000 cycling	17.2	[19]
Graphene–Cellulose Paper	–	120 (based on graphene mass, 1 mV/s)	99.1% after 5000 cycling	16.6	[14]
SWCNT/PANI nanoribbon	40.5 (polyaniline addition, 0.2 mA/cm ²)	–	79% after 1000 cycling	–	[61]
RGO/CNT aerogel	–	110 ^a (based on RGO + CNT)	80% after 10,000 cycling	–	[62]
Ti ₃ C ₂ Tx/CNF	22 ^b	84.6 (1 mA/cm ²)	85% after 5,000 cycling	–	[63]
ACFP-10	41.8 (0.5 mA/cm ²), 37.8 ^b	134.1 ^a	–	1786	This work
ACFP-15	24.1 (0.5 mA/cm ²), 22.0 ^b	80.0 ^a	100% after 10,000 cycling	1640	This work

- represents one not mentioned.

^a capacitance was measured at a current density of 0.4–1.0 A/g. (Based on the mass of entire electrode).

^b capacitance was measured at a current density of 2 mA/cm². (Based on the mass of entire electrode).

capacitance reached $1.2\text{F}/\text{cm}^2$ and current density was $0.5\text{ mA}/\text{cm}^2$, which was much higher than the original unloaded specific capacitance (Fig. S15c). Therefore, ACFPs can also be served as a superior substrate material for pseudocapacitor, which is conducive to the further improvement of specific capacitance.

Furthermore, the thickness of ACFP-15 was only $112\text{ }\mu\text{m}$, which was prepared by primary CP (15% CF) with grammage of $80\text{ g}/\text{m}^2$ through continuous carbonization and activation process. While the grammage of primary CP (15% CF) increased, thicker ACFP-15 will be prepared correspondingly. This means that there is still more space can be expansion of the current ACFPs electrode to further improve its capacitance by fabricating thicker ACFPs or depositing extra active materials in subsequent treatment. Of course, the basis of all is that ACFPs should integrate the characteristics of high SSA, high conductivity and flexible mechanical properties, which will facilitate the large-scale application of ACFPs in paper-based electrode materials.

4. Conclusions

In summary, this work demonstrated the effectiveness of a facile and economical strategy by using pulp fibers and CFs to prepare cellulose-based ACFPs with high electrical conductivity, electrochemical performance, and flexible mechanical properties. The synergistic effect of CFs addition and H_3PO_4 impregnation enabled the primary CPs to maintain remarkable mechanical properties after thermal carbonization and double activation. In the ACFPs, the transformed ACFs matrix from fibrillated pulp fibers were served as the main place for ACFPs ion energy storage. While the CFs proved to be the conductive skeleton material of ACFPs due to its low thermal expansion coefficient and excellent conductivity. This unique design provided higher specific capacitance and superior cycle stability of ACFP than most carbon-based paper electrode materials. Moreover, the cellulose-based ACFPs were readily augmented with pseudocapacitive materials for enhanced capacitance. On the whole, this study proposes a scalable approach to prepare low-cost, high-performance paper-based electrode which develop a broad development prospect in the field of energy storage.

Declaration of Competing Interest

The authors declare that they have no known competing financial interests or personal relationships that could have appeared to influence the work reported in this paper.

Data availability

The authors do not have permission to share data.

Acknowledgments

The authors acknowledge Guangdong Basic and Applied Basic Research Foundation (2019B151502043), and the China Scholarships Council (CSC No.202106150082).

Appendix A. Supplementary data

Supplementary data to this article can be found online at <https://doi.org/10.1016/j.cej.2022.137938>.

References

- [1] X. Zhao, Z. Xiong, Z. Qiao, X. Bo, D. Pang, J. Sun, J. Bian, Robust and flexible wearable generator driven by water evaporation for sustainable and portable self-power supply, *Chem. Eng. J.* 434 (2022), <https://doi.org/10.1016/j.cej.2022.134671>.
- [2] J. Liang, C. Jiang, W. Wu, Toward fiber-, paper-, and foam-based flexible solid-state supercapacitors: electrode materials and device designs, *Nanoscale* 11 (15) (2019) 7041–7061, <https://doi.org/10.1039/c8nr10301a>.
- [3] J. Liang, B. Tian, S. Li, C. Jiang, W. Wu, All-printed MnHCF-MnOx-based high-performance flexible supercapacitors, *Adv. Energy Mater.* 10 (12) (2020), <https://doi.org/10.1002/aenm.202000022>.
- [4] M. Wagih, A. Komolafe, N. Hillier, Screen-printable flexible textile-based ultra-broadband millimeter-wave DC-blocking transmission lines based on microstrip-embedded printed capacitors, *IEEE J. Microwaves* 2 (1) (2022) 162–173, <https://doi.org/10.1109/jmw.2021.3126927>.
- [5] Q. Huang, Y. Yang, R. Chen, X. Wang, High performance fully paper-based all-solid-state supercapacitor fabricated by a papermaking process with silver nanoparticles and reduced graphene oxide-modified pulp fibers, *EcoMat* 3 (1) (2021), <https://doi.org/10.1002/eom2.12076>.
- [6] Y.Z. Zhang, Y. Wang, T. Cheng, W.Y. Lai, H. Pang, W. Huang, Flexible supercapacitors based on paper substrates: a new paradigm for low-cost energy storage, *Chem. Soc. Rev.* 44 (15) (2015) 5181–5199, <https://doi.org/10.1039/c5cs00174a>.
- [7] Z. Wang, P. Tammela, M. Strømme, L. Nyholm, Cellulose-based supercapacitors: material and performance considerations, *Adv. Energy Mater.* 7 (18) (2017), <https://doi.org/10.1002/aenm.201700130>.
- [8] D. Zhao, Y. Zhu, W. Cheng, W. Chen, Y. Wu, H. Yu, Cellulose: Cellulose-Based Flexible Functional Materials for Emerging Intelligent Electronics (Adv. Mater. 28/2021), *Advanced Materials* 33(28) (2021) 2170213, [10.1002/adma.202170213](https://doi.org/10.1002/adma.202170213).
- [9] Z. Wang, Y.-H. Lee, S.-W. Kim, J.-Y. Seo, S.-Y. Lee, L. Nyholm, Why cellulose-based electrochemical energy storage devices? *Adv. Mater.* 33 (28) (2021) 2000892, <https://doi.org/10.1002/adma.202000892>.
- [10] M.M. Pérez-Madrigal, M.G. Edo, C. Aleman, Powering the future: application of cellulose-based materials for supercapacitors, *Green Chem.* 18 (22) (2016) 5930–5956, <https://doi.org/10.1039/c6gc02086k>.
- [11] H. Wu, J. Bi, Y. Li, L. Wang, X. Pang, C. Xiong, Z. Li, Low-cost and low-density carbonized facial tissue supported uniform NiCo2S4 nanotubes for high capacity flexible solid-state supercapacitors, *J. Materiomics* 7 (1) (2021) 166–176, <https://doi.org/10.1016/j.jmat.2020.06.011>.
- [12] L. Dong, C. Xu, Y. Li, Z. Pan, G. Liang, E. Zhou, F. Kang, Q.-H. Yang, Breathable and wearable energy storage based on highly flexible paper electrodes, *Adv. Mater.* 28 (42) (2016) 9313–9319, <https://doi.org/10.1002/adma.201602541>.
- [13] L. Yuan, B. Yao, B. Hu, K. Huo, W. Chen, J. Zhou, Polypyrrole-coated paper for flexible solid-state energy storage, *Energy Environ. Sci.* 6 (2) (2013), <https://doi.org/10.1039/c2ee23977a>.
- [14] Z. Weng, Y. Su, D.-W. Wang, F. Li, J. Du, H.-M. Cheng, Graphene-cellulose paper flexible supercapacitors, *Adv. Energy Mater.* 1 (5) (2011) 917–922, <https://doi.org/10.1002/aenm.201100312>.
- [15] S. Li, D. Huang, J. Yang, B. Zhang, X. Zhang, G. Yang, M. Wang, Y. Shen, Freestanding bacterial cellulose-polypyrrole nanofibres paper electrodes for advanced energy storage devices, *Nano Energy* 9 (2014) 309–317, <https://doi.org/10.1016/j.nanoen.2014.08.004>.
- [16] L. Hu, J.W. Choi, Y. Yang, S. Jeong, F. La Mantia, L.-F. Cui, Y. Cui, Highly conductive paper for energy-storage devices, *Proc. Natl. Acad. Sci.* 106 (51) (2009) 21490–21494.
- [17] G. Zheng, L. Hu, H. Wu, X. Xie, Y. Cui, Paper supercapacitors by a solvent-free drawing method, *Energy Environ. Sci.* 4 (9) (2011), <https://doi.org/10.1039/c1ee01853a>.
- [18] W. Tian, A. VahidMohammadi, M.S. Reid, Z. Wang, L. Ouyang, J. Erlandsson, T. Pettersson, L. Wågberg, M. Beidaghi, M.M. Hamed, Multifunctional nanocomposites with high strength and capacitance using 2D MXene and 1D nanocellulose, *Adv. Mater.* 31 (41) (2019) 1902977, <https://doi.org/10.1002/adma.201902977>.
- [19] J. Bi, H. Wu, L. Wang, X. Pang, Y. Li, Q. Meng, L. Wang, A mass production paper-making method to prepare superior flexible electrodes and asymmetric supercapacitors with high volumetric capacitance, *Electrochim. Acta* 367 (2021), <https://doi.org/10.1016/j.electacta.2020.137409>.
- [20] X. Wu, M. Zhang, T. Song, H. Mou, Z. Xiang, H. Qi, Highly durable and flexible paper electrode with a dual fiber matrix structure for high-performance supercapacitors, *ACS Appl. Mater. Interfaces* 12 (11) (2020) 13096–13106, <https://doi.org/10.1021/acsmami.9b19347>.
- [21] Y. Kuang, C. Chen, G. Pastel, Y. Li, J. Song, R. Mi, W. Kong, B. Liu, Y. Jiang, K. Yang, L. Hu, Conductive cellulose nanofiber enabled thick electrode for compact and flexible energy storage devices, *Adv. Energy Mater.* 8 (33) (2018) 1802398, <https://doi.org/10.1002/aenm.201802398>.
- [22] S. Zhou, X. Kong, B. Zheng, F. Huo, M. Stromme, C. Xu, Cellulose nanofiber @ conductive metal-organic frameworks for high-performance flexible supercapacitors, *ACS Nano* 13 (8) (2019) 9578–9586, <https://doi.org/10.1021/acsnano.9b04670>.
- [23] H. Chen, T. Liu, J. Mou, W. Zhang, Z. Jiang, J. Liu, J. Huang, M. Liu, Free-standing N-self-doped carbon nanofiber aerogels for high-performance all-solid-state supercapacitors, *Nano Energy* 63 (2019), <https://doi.org/10.1016/j.nanoen.2019.06.032>.
- [24] J. Du, L. Liu, Z. Hu, Y. Yu, Y. Zhang, S. Hou, A. Chen, Raw-cotton-derived n-doped carbon fiber aerogel as an efficient electrode for electrochemical capacitors, *ACS Sustain. Chem. Eng.* 6 (3) (2018) 4008–4015, <https://doi.org/10.1021/acssuschemeng.7b04396>.
- [25] T. Zhang, Z. Mao, X. Shi, J. Jin, B. He, R. Wang, Y. Gong, H. Wang, Tissue-derived carbon microbelt paper: a high-initial-coulombic-efficiency and low-discharge-platform K+-storage anode for 4.5 V hybrid capacitors, *Energy & Environmental Science* 15(1) (2022) 158–168, [10.1039/dle03214c](https://doi.org/10.1039/dle03214c).
- [26] C. Hu, Y. He, S. Chen, Y. Zhu, M. Hanif, H. Hou, Binder-free activated carbon papers for high-performance electric double-layer capacitors, *J. Solid State*

- Electrochem. 18 (10) (2014) 2797–2802, <https://doi.org/10.1007/s10008-014-2535-7>.
- [27] P. Morgan, Carbon fibers and their composites, CRC press2005.
- [28] C. Soutis, Fibre reinforced composites in aircraft construction, Prog. Aerosp. Sci. 41 (2) (2005) 143–151, <https://doi.org/10.1016/j.paerosci.2005.02.004>.
- [29] D.S. Cousins, Y. Suzuki, R.E. Murray, J.R. Samaniuk, A.P. Stebner, Recycling glass fiber thermoplastic composites from wind turbine blades, J. Cleaner Prod. 209 (2019) 1252–1263, <https://doi.org/10.1016/j.jclepro.2018.10.286>.
- [30] C. Zhao, Y. Hu, Y. Zhou, N. Li, Y. Ding, J. Guo, C. Zhao, Y. Yang, Aerobic recovered carbon fiber support-based MoO₂/MnO₂ asymmetric supercapacitor with a widened voltage window, Energy Fuels 35 (8) (2021) 6909–6920, <https://doi.org/10.1021/acs.energyfuels.1c00682>.
- [31] S. Geng, T. Zhou, M. Jia, X. Shen, P. Gao, S. Tian, P. Zhou, B. Liu, J. Zhou, S. Zhuo, F. Li, Carbon-coated WS₂ nanosheets supported on carbon nanofibers for high-rate potassium-ion capacitors, Energy Environ. Sci. 14 (5) (2021) 3184–3193, <https://doi.org/10.1039/dlee00193k>.
- [32] Z. Wang, Y. Han, Y. Zeng, Y. Qie, Y. Wang, D. Zheng, X. Lu, Y. Tong, Activated carbon fiber paper with exceptional capacitive performance as a robust electrode for supercapacitors, J. Mater. Chem. A 4 (16) (2016) 5828–5833, <https://doi.org/10.1039/c6ta02056a>.
- [33] M. Sawangphruk, P. Srimuk, P. Chiochan, A. Krittayavathananon, S. Luanwuthi, J. Limtrakul, High-performance supercapacitor of manganese oxide/reduced graphene oxide nanocomposite coated on flexible carbon fiber paper, Carbon 60 (2013) 109–116, <https://doi.org/10.1016/j.carbon.2013.03.062>.
- [34] P. Srimuk, S. Luanwuthi, A. Krittayavathananon, M. Sawangphruk, Solid-type supercapacitor of reduced graphene oxide-metal organic framework composite coated on carbon fiber paper, Electrochim. Acta 157 (2015) 69–77, <https://doi.org/10.1016/j.electacta.2015.01.082>.
- [35] H. Li, J. Liang, H. Li, X. Zheng, Y. Tao, Z.-H. Huang, Q.-H. Yang, Activated carbon fibers with manganese dioxide coating for flexible fiber supercapacitors with high capacitive performance, J. Energy Chem. 31 (2019) 95–100, <https://doi.org/10.1016/j.jechem.2018.05.008>.
- [36] Y. Zhu, S. Cheng, W. Zhou, J. Jia, L. Yang, M. Yao, M. Wang, P. Wu, H. Luo, M. Liu, Porous functionalized self-standing carbon fiber paper electrodes for high-performance capacitive energy storage, ACS Appl Mater Interfaces 9 (15) (2017) 13173–13180, <https://doi.org/10.1021/acsmami.7b01210>.
- [37] T.D. Burchell, J.Y. Chen, C.I. Contescu, J. Economy, N.C. Gallego, S. Giraudet, H. A. Grappe, A. Hassani, Y. Huang, A. Javid, G. Jiang, V. Jiménez, A.R. Khataee, P. Le Cloirec, Q.W. Li, Y. Li, A. Romero, D. Saha, P. Sánchez, Y. Shen, Z. Yue, X. H. Zhang, M. Zhang, Contributors, in: J.Y. Chen (Ed.), Activated Carbon Fiber and Textiles, Woodhead Publishing, Oxford, 2017, pp. ix–x.
- [38] M. Suzuki, Activated carbon fiber: fundamentals and applications, Carbon 32 (4) (1994) 577–586.
- [39] S. Sharma, S.S. Nair, Z. Zhang, A.J. Ragauskas, Y. Deng, Characterization of micro fibrillation process of cellulose and mercerized cellulose pulp, RSC Adv. 5 (77) (2015) 63111–63122, <https://doi.org/10.1039/c5ra09068g>.
- [40] S. Gharehkhani, E. Sadeghinezhad, S.N. Kazi, H. Yarmand, A. Badarudin, M. R. Safaei, M.N. Zubir, Basic effects of pulp refining on fiber properties—a review, Carbohydr Polym 115 (2015) 785–803, <https://doi.org/10.1016/j.carbpol.2014.08.047>.
- [41] M. Jagtoyen, F. Derbyshire, Activated carbons from yellow poplar and white oak by H₃PO₄ activation, Carbon 36 (7–8) (1998) 1085–1097.
- [42] J.M. Rosas, R. Ruiz-Rosas, J. Rodríguez-Mirasol, T. Cordero, Kinetic study of the oxidation resistance of phosphorus-containing activated carbons, Carbon 50 (4) (2012) 1523–1537, <https://doi.org/10.1016/j.carbon.2011.11.030>.
- [43] P. Williams, A. Reed, Development of activated carbon pore structure via physical and chemical activation of biomass fibre waste, Biomass Bioenergy 30 (2) (2006) 144–152, <https://doi.org/10.1016/j.biombioe.2005.11.006>.
- [44] C. Lee, K. Dazen, K. Kafle, A. Moore, D.K. Johnson, S. Park, S.H. Kim, Correlations of apparent cellulose crystallinity determined by XRD, in: NMR, IR, Raman, and SFG Methods, in: O.J. Rojas, (Ed.), Cellulose Chemistry and Properties: Fibers, Nanocelluloses and Advanced Materials, Springer International Publishing, Cham, 2016, pp. 115–131, https://doi.org/10.1007/12_2015_320.
- [45] A.D. French, Idealized powder diffraction patterns for cellulose polymorphs, Cellulose 21 (2) (2013) 885–896, <https://doi.org/10.1007/s10570-013-0030-4>.
- [46] K. Hina, H. Zou, W. Qian, D. Zuo, C. Yi, Preparation and performance comparison of cellulose-based activated carbon fibres, Cellulose 25 (1) (2017) 607–617, <https://doi.org/10.1007/s10570-017-1560-y>.
- [47] M. Jian-feng, Y. Shu-min, T. Gen-lin, L. Xing-e, Study on the Application of Raman Spectroscopy to the Research on Natural Cellulose Structure, Guang pu xue yu guang pu fen xi = Guang pu 36 (2016) 1734–1739.
- [48] A.C. Ferrari, J. Robertson, Interpretation of Raman spectra of disordered and amorphous carbon, Phys. Rev. B 61 (20) (2000) 14095–14107, <https://doi.org/10.1103/PhysRevB.61.14095>.
- [49] L. Zhao, W. Zheng, O. Mašek, X. Chen, B. Gu, B.K. Sharma, X. Cao, Roles of phosphoric acid in biochar formation: synchronously improving carbon retention and sorption capacity, J. Environ. Qual. 46 (2) (2017) 393–401.
- [50] K.M. Khalil, W.A. Elhamdy, K.M. Mohammed, A.-E.-A.-A. Said, Nanostructured P-doped activated carbon with improved mesoporous texture derived from biomass for enhanced adsorption of industrial cationic dye contaminants, Mater. Chem. Phys. 282 (2022), 125881.
- [51] A.M. Puziy, O.I. Poddubnaya, R.P. Socha, J. Gurgul, M. Wisniewski, XPS and NMR studies of phosphoric acid activated carbons, Carbon 46 (15) (2008) 2113–2123, <https://doi.org/10.1016/j.carbon.2008.09.010>.
- [52] Y.-F. Wang, S.-L. Zuo, Electrochemical properties of phosphorus-containing activated carbon electrodes on electrical double-layer capacitors, Acta Phys. Chim. Sin. 32 (2) (2016) 481–492, <https://doi.org/10.3866/pku.Whxb201511041>.
- [53] L. Liu, Z. Niu, L. Zhang, W. Zhou, X. Chen, S. Xie, Nanostructured graphene composite papers for highly flexible and foldable supercapacitors, Adv. Mater. 26 (28) (2014) 4855–4862, <https://doi.org/10.1002/adma.201401513>.
- [54] X. Zhang, Z. Lin, B. Chen, S. Sharma, C.-P. Wong, W. Zhang, Y. Deng, Solid-state, flexible, high strength paper-based supercapacitors, J. Mater. Chem. A 1 (19) (2013), <https://doi.org/10.1039/c3ta10827a>.
- [55] J. Chen, H. Li, L. Zhang, C. Du, T. Fang, J. Hu, Direct reduction of graphene oxide/nanofibrillated cellulose composite film and its electrical conductivity research, Sci. Rep. 10 (1) (2020) 3124, <https://doi.org/10.1038/s41598-020-59918-z>.
- [56] R. Chen, H. Ling, Q. Huang, Y. Yang, X. Wang, Interface engineering on cellulose-based flexible electrode enables high mass loading wearable supercapacitor with ultrahigh capacitance and energy density, Small 18 (9) (2022) 2106356, <https://doi.org/10.1002/smll.202106356>.
- [57] H. Banda, S. Périé, B. Daffos, L. Dubois, O. Crosnier, P. Simon, P.-L. Taberna, F. Duclairoir, Investigation of ion transport in chemically tuned pillared graphene materials through electrochemical impedance analysis, Electrochim. Acta 296 (2019) 882–890, <https://doi.org/10.1016/j.electacta.2018.11.122>.
- [58] S. Yuan, X. Huang, H. Wang, L. Xie, J. Cheng, Q. Kong, G. Sun, C.-M. Chen, Structure evolution of oxygen removal from porous carbon for optimizing supercapacitor performance, J. Energy Chem. 51 (2020) 396–404, <https://doi.org/10.1016/j.jechem.2020.04.004>.
- [59] R. Chen, Y. Yang, Q. Huang, H. Ling, X. Li, J. Ren, K. Zhang, R. Sun, X. Wang, A multifunctional interface design on cellulose substrate enables high performance flexible all-solid-state supercapacitors, Energy Storage Mater. 32 (2020) 208–215, <https://doi.org/10.1016/j.ensm.2020.07.030>.
- [60] S. Li, D. Huang, B. Zhang, X. Xu, M. Wang, G. Yang, Y. Shen, Flexible supercapacitors based on bacterial cellulose paper electrodes, Adv. Energy Mater. 4 (10) (2014), <https://doi.org/10.1002/aenm.201301655>.
- [61] D. Ge, L. Yang, L. Fan, C. Zhang, X. Xiao, Y. Gogotsi, S. Yang, Foldable supercapacitors from triple networks of macroporous cellulose fibers, single-walled carbon nanotubes and polyaniline nanoribbons, Nano Energy 11 (2015) 568–578, <https://doi.org/10.1016/j.nanoen.2014.11.023>.
- [62] O. Okhay, A. Tkach, M.J.H. Gallo, G. Otero-Irueta, S. Mikhalev, P. Staiti, F. Lufrano, Energy storage of supercapacitor electrodes on carbon cloth enhanced by graphene oxide aerogel reducing conditions, J. Storage Mater. 32 (2020), <https://doi.org/10.1016/j.est.2020.101839>.
- [63] W. Chen, D. Zhang, K. Yang, M. Luo, P. Yang, X. Zhou, Mxene (Ti₃C₂T)/cellulose nanofiber/porous carbon film as free-standing electrode for ultrathin and flexible supercapacitors, Chem. Eng. J. 413 (2021), <https://doi.org/10.1016/j.cej.2020.127524>.